# Supporting Information

## Frequency-dependent selectively oriented edge states topological transport

Jiajun Ma[1], Chunmei Ouyang[1,*], Yuting Yang[2,*], Xinyue Qian[2], Li Niu[1], Yi Liu[1], Quan Xu[1], Yanfeng Li[1], Zhen Tian[1], Jianqiang Gu[1], Jiaguang Han[1, 3], and Weili Zhang[4,*]

[1]Center for Terahertz Waves and College of Precision Instrument and Optoelectronics Engineering, and the Key Laboratory of Optoelectronics Information and Technology, Tianjin University, Tianjin 300072, China

[2]School of Materials Science and Physics, China University of Mining and Technology, Xuzhou 221116, China

[3]Guangxi Key Laboratory of Optoelectronic Information Processing, School of Optoelectronic Engineering, Guilin University of Electronic Technology, Guilin 541004, China

[4]School of Electrical and Computer Engineering, Oklahoma State University Stillwater, Oklahoma 74078, USA

Corresponding authors:

cmouyang@tju.edu.cn; yangyt@cumt.edu.cn; weili.zhang@okstate.edu

## 1. Dispersion relations of a ribbon-shaped supercell.

Using the commercial finite element method-based software COMSOL Multiphysics, we calculate the dispersion relations of a ribbon-shaped supercell consisting of valley photonic crystals (VPCs). Two cases are considered where the supercell has inversion symmetry and has no inversion symmetry by tuning the height difference or adjusting the radius difference, as displayed in Fig. S1. Figure S1a shows that there is PBG2 when the VPCs comprising the supercell have inversion symmetry ($\Delta h = 0$ and $\Delta r = 0$). When the height difference ($\Delta h \neq 0$ and $\Delta r = 0$) is tuned or the radius difference ($\Delta h = 0$ and $\Delta r \neq 0$) is adjusted to break the inversion symmetry of the VPCs, PBG2 is always present, as shown in Figs. S1b and c, respectively. It can be concluded that PBG2 has no relationship with the perturbation Δ, and whether the VPCs break the inversion symmetry or not, the supercells will always have PBG2.

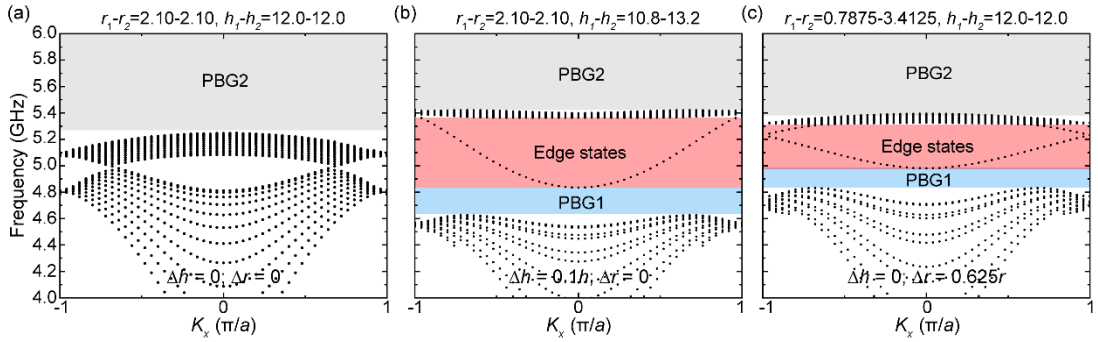


**Figure S1. Dispersion relations of the ribbon-shaped supercell consisting of VPCs**, when the supercell has inversion symmetry (a) and has no inversion symmetry by tuning the height difference (b) or adjusting the radius difference (c). The purple and gray shaded areas denote the edge states and the photonic bandgaps (PBGs) of the supercells, respectively. $K_x$ denotes the wavevector along the domain wall of the two VPCs.

## 2. Theoretical proof that PBG is governed by the perturbation in valley TPCs.

On the basis of Maxwell's equations, we consider harmonic transverse magnetic (TM) modes of electromagnetic waves. The master equation for a photonic crystal can be expressed as: $\nabla^2 E_z(\vec{r}) + [\bar{\varepsilon} + \Delta\bar{\varepsilon}(\vec{r})]\left(\frac{\omega}{c}\right)^2 E_z(\vec{r}) = 0$, where $E_z(\vec{r})$ represents the electric field, $\omega$ is the angular frequency, $c$ is the speed of light, $\varepsilon(\vec{r})$ is the permittivity associated with the position vector $\vec{r}$, $\bar{\varepsilon}$ is the average relative permittivity, and $\Delta\bar{\varepsilon}(\vec{r})$ is the change of $\varepsilon(\vec{r})$ relative to $\bar{\varepsilon}$. It can be concluded that only when $\bar{\varepsilon}$ and $\Delta\bar{\varepsilon}(\vec{r})$ meet certain conditions will the electric field $E_z(\vec{r})$ be a solution within a certain range of the angular frequency $\omega$. In the case of no

solution, a PBG exists. Hence, the parameters affecting the PBG are $\bar{\varepsilon}$ and $\Delta\bar{\varepsilon}(\vec{r})$, the latter being determined by the difference in the dielectric constants of the two media.

The Hamiltonian describing the perturbed crystal near each of the K and K' valleys can be expressed as $H = \upsilon_D(\delta k_x \tau_z \sigma_x + \delta k_y \tau_0 \sigma_y) + m\tau_0\sigma_z$, where $v_D$ is the group velocity and $\delta k$ is the momentum relative to the K and K' points. The Pauli matrices $\tau_{x,y,z}$ and $\sigma_{x,y,z}$ act on the valley and orbital state vectors. The mass term $m$ is calculated by determining the change in the permittivity of the perturbed crystal.

Since $\Delta\bar{\varepsilon}(\vec{r})$ and the mass term $m$ are calculated by determining the change in the permittivity of the perturbed crystal and the change in the permittivity of the valley topological photonic crystals (TPCs) is governed by the perturbation Δ, it can be concluded that the PBG is determined by the perturbation Δ in the valley TPCs.

**3. TPC I and TPC II valley TPCs.**

To achieve valley TPCs with different working frequency ranges, we consider TPC I and TPC II valley TPCs consisting of aluminum rods of different heights and radii. As displayed in Fig. S2a, the geometric parameters are as follows: the lattice constant is $a$ = 14 mm; in the TPC I lattice, the height of rod 1 (rod 2) is $h_1$ = 11.6 mm ($h_2$ = 12.7 mm), and the radius of rod 1 (rod 2) is $r_1$ = 1.05 mm ($r_2$ = 3.15 mm); in the TPC II lattice, the height of rod 1 (rod 2) is $h_3$ = 12.4 mm ($h_4$ = 13.8 mm), and the radius of rod 1 (rod 2) is $r_1$ = 1.05 mm ($r_2$ = 3.15 mm). When these two rods have a uniform height and radius (that is, TPC I: $h = h_1 = h_2$ = 12.15 mm, and $r = r_1 = r_2 = 0.15a$ = 2.1 mm; TPC II: $h = h_3 = h_4$ = 13.10 mm, and $r = r_1 = r_2 = 0.15a$ = 2.1 mm), the band structures in Fig. S2b show Dirac dispersions near the K (K') points of the Brillouin zone at 5.18 and 4.82 GHz, respectively. Then by simultaneously changing the ratio of the rod radii $r_1/r_2$ and inducing the difference of the rod heights $h_1$-$h_2$ to break the inversion symmetry, complete PBGs (4.83 GHz < $f_1$ < 5.61 GHz for TPC I and 4.48 GHz < $f_2$ < 5.34 GHz for TPC II) can be achieved.

We numerically calculate the dispersion relations of ribbon-shaped supercells and transmission spectra of straight waveguides to obtain the working frequencies of TPC I and TPC II, and the dispersion relations of the edge states for TPC I and TPC II are marked by the blue and red lines in Fig. S2c, respectively. The bandwidths of the valley edge states in TPC I and TPC II are 4.81–5.31 GHz and 5.03–5.59 GHz, respectively, and PBGs appear between the edge and lower bulk states for TPC I and TPC II. To

determine the bandwidth of the PBGs, the simulated transmission spectra for both TPC I (blue line) and TPC II (red line) are shown in Fig. S2D. The simulated transmission spectra of the straight waveguides in Fig. S2d agree well with the calculated band diagrams for the ribbon-shaped supercells in Fig. S2c. For TPC I, the bandwidths of PBG2 and edge states are 4.78–5.03 GHz and 5.03–5.59 GHz, respectively. For TPC II, the bandwidths of PBG2 and edge states are 4.48–4.81 GHz and 4.81–5.31 GHz, respectively. Within the frequency range of the edge states, high transmission is preserved when the excited edge states go along the domain walls. To further directly image the robust transmission, the simulated $E_z$ fields of TPC I at 5.41 GHz and of TPC II at 4.92 GHz are shown in Fig. S2e, where it can be seen that the edge states pass along the straight domain walls and robust valley edge transport is demonstrated.

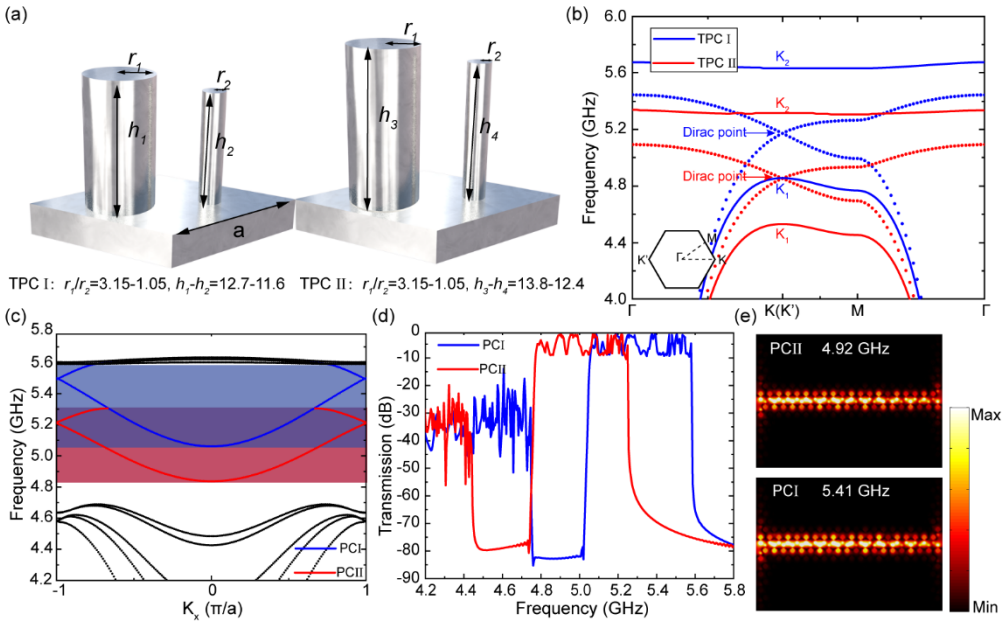


**Figure S2. (**a) Schematic of TPC I and TPC II, where the rhomboidal unit cell consists of two inequivalent metallic rods with different radii and heights on top of a metal surface. (b) Band diagrams with and without inversion symmetry. (c) Dispersion relations of the valley-dependent edge states of TPC I and TPC II. (d) Simulated transmission spectra of TPC I and TPC II straight waveguides. (e) Simulated $E_z$ field profiles in the *xy* planes of TPC I at 5.41 THz and of TPC II at 4.92 THz.

**4. The armchair domain wall along the *y*-axis in the FSDT device.**

For the FSDT topological photonic devices, there is another armchair domain wall (orange line) between TPC I and TPC II along the *y*-axis in Fig. S3a. Here the only difference between the two TPCs is the different heights of the rods (TPC I: $h_{rod1}$=11.6 mm and $h_{rod2}$=12.7 mm; TPC II: $h_{rod1}$=12.4 mm and $h_{rod2}$=13.8 mm), and the valley

Chern indices near K(K') for the first band of TPC I and TPC II are the same ($C_K$=+1/2 ($C_{K'}$=–1/2)), resulting in the valley Chern number near K(K') across the armchair domain wall being $\Delta C^{K(K')} = C_{left}^{K(K')} - C_{right}^{K(K')} = 0$. According to the bulk-boundary correspondence, no topological edge states will emerge. The dispersion curves in Fig. S3b show that there are no edge states in the PBG, and the armchair domain wall does not support topological interface modes.

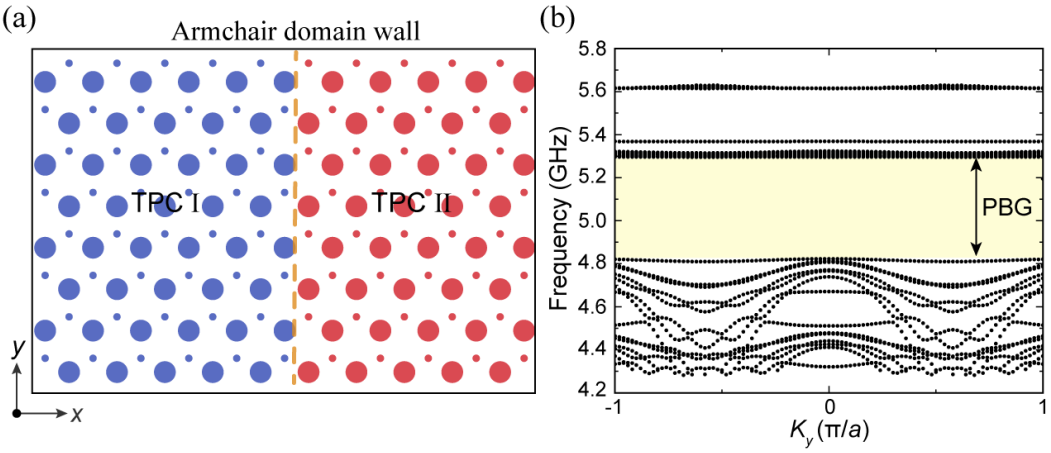


**Figure S3** (a) Schematic of the armchair domain wall formed between TPC I and TPC II along the *y*-axis. (b) Dispersion curves of the supercell for the armchair domain wall.

**5. FSDT device with valley TPCs where the topological edge states and bulk states are continuous.**

If we use the previously described VPCs where the topological edge states and bulk states are continuous, the WDM and ADM functions of an FSDT device cannot be achieved. Because the edge states and lower bulk states are continuous, the LF regime corresponds to both the valley edge states of TPC II and the bulk states of TPC I. Hence, the LF EM waves not only transmit one way along the domain wall of TPC II, but also propagate into the TPC I body, as shown in Fig. S4.

To demonstrate the functions of the FSDT device, we fabricate a finite-sized sample consisting of 20 × 16 unit cells, as depicted in Fig. S5a. The transmission spectra and field distributions are simulated with CST Microwave Studio. The valley edge states can be excited at ports S2, S3 and S4, and the detection probe can be located at ports S1 and S5. The receiver placed at ports 1 and 5 can accept EM waves that transmit along the domain walls of TPC I and TPC II, respectively. The simulated transmission spectra and field distributions in Figs. S5b, c and d show that the IF (4.90–5.30 GHz) and HF (5.30–5.60 GHz) EM waves can achieve the functions of the FSDT device, but

the LF (4.60–4.90 GHz) EM waves cannot because they will propagate into the TPC I body. Therefore, the valley TPCs with PBGs, as we proposed, are necessary to realize the FSDT device.

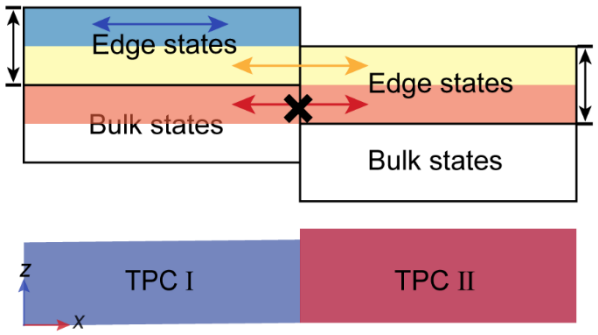


**Figure S4.** Design method for the FSDT device using valley TPCs where the topological edge states and bulk states are continuous.

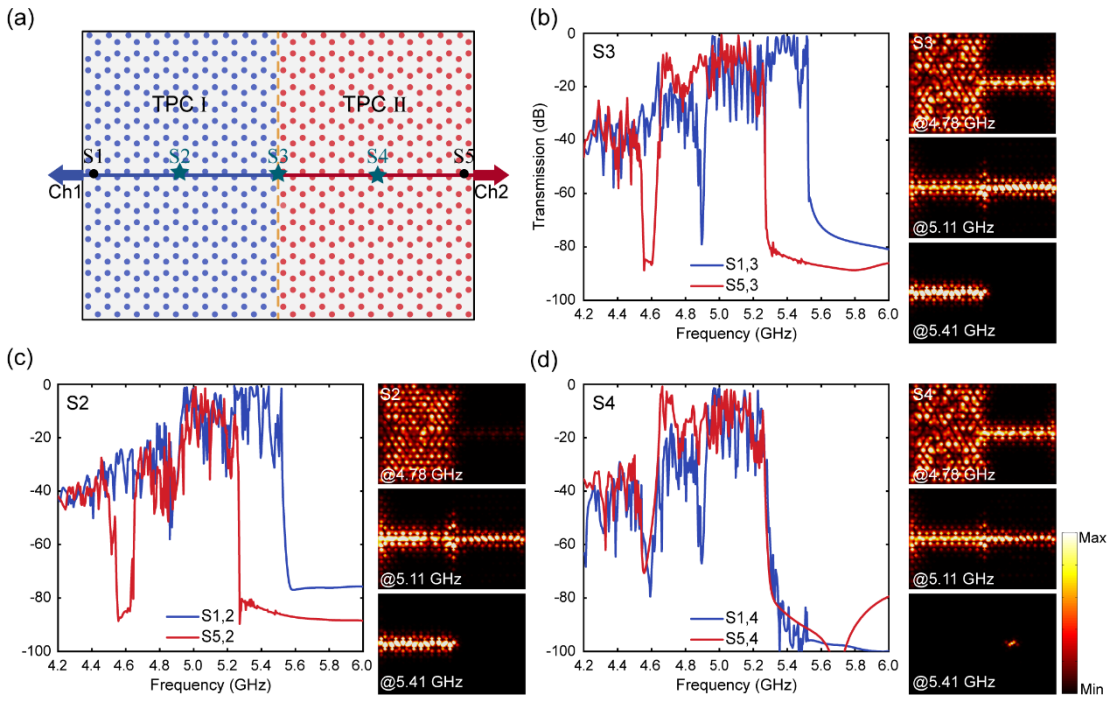


**Figure S5.** (a) Schematic of the FSDT topological photonic device, which is composed of valley TPCs where the topological edge states and bulk states are continuous. (b, c, d) Simulated transmission spectra (in dB) when the source is placed at ports S3, S2 and S4 to achieve the WDM and ADM functions, respectively. The insets on the right are the experimental $E_z$ field intensity distributions of the edge states at 4.88, 5.13, and 5.44 GHz, respectively.

## 6. The robustness of the edge states and FSDT device.

To verify the robustness of the topological edge states along the zigzag domain wall, we first design straight waveguides with no defects, local disorders and structural

defects, as shown in Fig. S6a. By comparing their transmission spectra (see Fig. S6b), it can be observed that the disorders and defects do not affect the transmission of EM waves. To further demonstrate the robustness of the FSDT topological photonic device, we then construct an FSDT device with four sharp bends, as illustrated in Fig. S7a. The transmission spectra and electric field distributions (Figs. S7(b-c)) show that the topological edge state can be guided around the zigzag path smoothly without reflection. Therefore, the edge states are immune to disorders, defects and sharp bends.

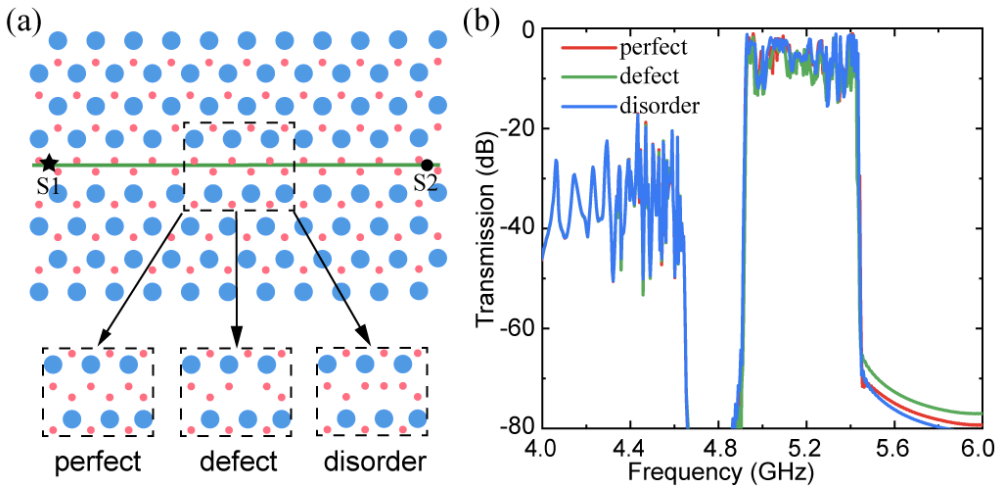


**Figure S6.** (a) Schematic of the zigzag interface in straight topological waveguides with no defects, defects and disorders. (b) Simulated transmission spectra (in dB) of the three straight topological waveguides.

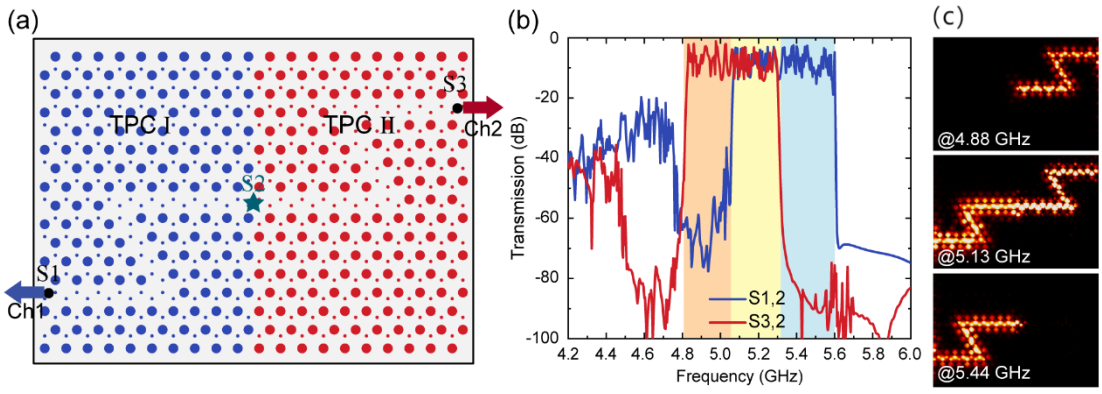


**Figure S7.** (a) Schematic of the FSDT topological photonic device with four sharp bends. (b) Simulated transmission spectra (in dB) at ports S1 and S3 when the source is placed at ports S2. (c) Simulated $E_z$ field distributions of the edge states at 4.88, 5.13, and 5.44 GHz (from top to bottom).

## 7. Simulation results of the multifunctional FSDT device.

To demonstrate the functions of the FSDT device that combines TPC I and TPC II, we simulate the transmission spectra and field distributions with CST Microwave Studio. The simulated spectrum when the source is located at port 3 to realize the WDM function is shown in Fig. S8b, where the IF and HF electromagnetic waves between 5.09–5.61 GHz propagate to the left along the domain wall of TPC I, and the LF and IF electromagnetic waves between 4.83–5.34 GHz transmit to the right along the domain wall of TPC II. The simulated $E_z$ electric field distributions at 4.88 GHz, 5.13 GHz, and 5.44 GHz show that the 5.44 GHz HF EM waves unidirectionally propagate to the left along the domain wall of TPC I; the 5.13 GHz IF EM waves bidirectionally propagate along the domain walls of TPC I and TPC II; and the 4.88 GHz LF EM waves transmit one way to the right along the domain wall of TPC II. The simulated transmission spectra and $E_z$ electric field distributions when the source is located at port 2 and port 4 are depicted in Figs. S8c and d, respectively, indicate the ADM function. When the excitation source is placed at port 2, the detection receiver at port 1 and port 5 accepts the IF and HF waves between 5.09–5.61 GHz and IF waves between 5.09–5.34 GHz, respectively. When the excitation source is placed at port 4, the detection receiver at port 1 and port 5 accepts the IF waves between 5.09–5.34 GHz and the LF and IF waves between 4.83–5.34 GHz, respectively.

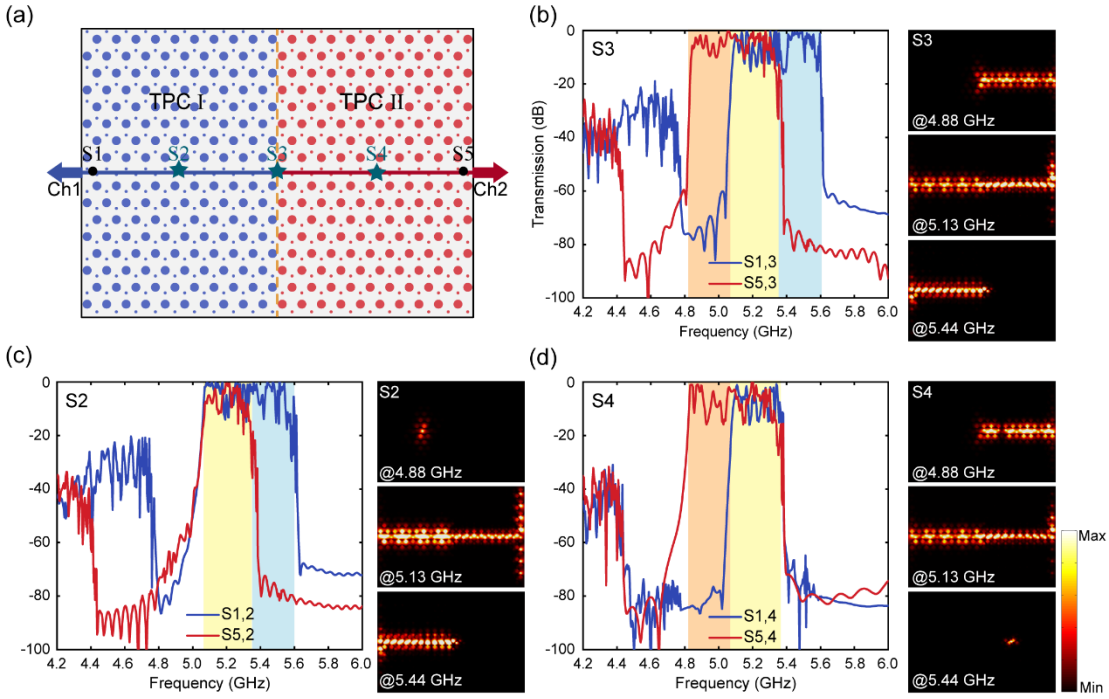


**Figure S8. (**a) Schematic of the topological photonic device, which is composed of TPC I and TPC II. The blue and red lines represent the positions of the domain walls of TPC I and TPC II, respectively. (b, c, d) Simulated transmission spectra (in dB) at ports S1 and S5 when the source

is placed at ports S3, S2, and S4, respectively. The transmission spectrum corresponding to port 1 is shown as the solid blue line, while that for port 5 is shown as the solid red line. The insets on the right in each figure are the simulated $E_z$ field distributions of the edge states at 4.88, 5.13, and 5.44 GHz (from top to bottom).